

CERN-TH-95-84  
SHEP 95-14

## SEARCH FOR LARGE RAPIDITY GAP EVENTS IN $e^+e^-$ ANNIHILATION

**John Ellis**

*Theoretical Physics Division, CERN*

*CH - 1211 Geneva 23*

and

**Douglas A. Ross**

*Physics Department, University of Southampton*

*Highfield, Southampton SO17 1BJ, England*

### ABSTRACT

We investigate the cross-section for the production of a low-mass colour-singlet cluster in  $e^+e^-$  annihilation with a large rapidity gap between the colour-singlet cluster and the other jets. It is argued that such events are the cross-channel analogue of large-rapidity-gap events in deep-inelastic scattering, and therefore could in principle be used to investigate the analytic continuation of the BFKL pomeron to the positive- $t$  kinematic regime, where one would expect the trajectory to pass through glueball states. The cross section can be calculated in perturbative QCD, so that the infrared scale arising from non-perturbative effects, which prevents an exponential fall-off with rapidity gap in the case of deep-inelastic scattering, is absent in  $e^+e^-$  annihilation. Correspondingly, the cross section for such events decreases rapidly with increasing rapidity gap.

CERN-TH-95-84  
SHEP 95-14  
4 April 1995

# 1 Introduction

The Pomeron is currently experiencing a renaissance, both theoretical - via several different perturbative approaches - and experimental - stimulated by observations at HERA. In the theoretical domain we mention in particular the BFKL Pomeron [1] obtained by summing perturbative logarithms in longitudinal momenta,  $x$ , and attempts to interpolate between the (BFKL) integral equation which describes this Pomeron and the GLAP evolution equation [2] which sums perturbative logarithms in transverse momenta,  $k_\perp$ . In the experimental domain we mention in particular the growth of the structure function at low values of Bjorken  $x$  and increasing  $Q^2$ , which may be a signal for the BFKL Pomeron, and the observation of deep inelastic final states with large rapidity gaps, which likewise may be revealing point-like structure within the Pomeron. <sup>†</sup>

The latter observations were preceded by the discovery of large  $p_\perp$  hadronic jets in large rapidity-gap events at the SPS  $p\bar{p}$  collider, which could be interpreted in terms of a hard point-like Pomeron structure function. These were followed by the observation of large rapidity-gaps in events with large  $p_\perp$  hadronic jets at the FNAL  $p\bar{p}$  collider. In view of the existence of large rapidity-gap events in  $ep$  and  $p\bar{p}$  collisions, it is natural to ask whether analogous events occur in high energy  $e^+e^-$  collisions. This question has been asked theoretically by Bjorken, Brodsky and Lu [4], who predicted a very small rate for large rapidity-gap events in  $Z$  decays, and indeed none have been reported by any experiment.

The purpose of this paper is to re-examine theoretically the possible existence of large rapidity-gap events in  $e^+e^-$  annihilation, building on the increased insight into the Pomeron provided by recent theoretical studies and HERA measurements. Large rapidity-gap events in  $e^+e^-$  annihilation would involve the production of an isolated cluster of hadrons that would in some sense constitute the direct channel ( $m^2 > 0$ ) analogue of the crossed channel ( $t < 0$ ) Pomeron. Indeed if the cluster were a single particle this would probably be a glueball state which lies on the Pomeron trajectory for positive  $t$ . The relation between these time-like and space-like regions may cast new light on both perturbative and non-perturbative aspects of the Pomeron.

The basic mechanism of the HERA large rapidity-gap events is illustrated in Fig.1. A photon of high virtuality  $Q \equiv \sqrt{-q^2}$  strikes a proton, producing a hadronic system of large mass  $W = \sqrt{(q+p)^2}$ , that comprises of two components - an undetected proton fragment separated by a large rapidity

---

<sup>†</sup>We emphasize here that the structure functions at low  $x$  are related by the optical theorem to the imaginary part of a single Pomeron exchange amplitude, whereas in the case of events with large rapidity-gaps it is the *amplitude* that is dominated by Pomeron exchange.

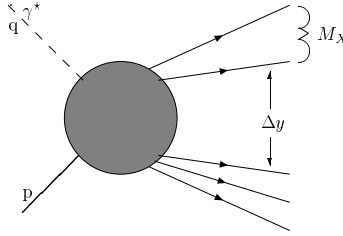


Figure 1: Rapidity-gap events in  $ep$  scattering.

gap ( $\Delta y$ ) from a hadronic cluster of mass,  $M_X$ . Such final states appear to constitute a finite fraction of the total deep-inelastic structure function,  $F_2$  in the double scaling limit,  $W/Q = 1/x - 1 \rightarrow \infty$ ,  $M_X/Q = 1/\beta - 1$  fixed, and  $Q \rightarrow \infty$ . In Regge lore

$$F_2(x, Q) \propto \left(\frac{1}{x}\right)^{\alpha_P(0)-1}$$

at small  $x$  and  $Q$  fixed, where  $\alpha_P(t)$  is the Pomeron trajectory which is treated here as a simple Regge pole. The contribution of large rapidity gap events would be parametrized in this framework as

$$F_2^{LRG}(x, Q) \propto \left(\frac{1}{x}\right)^{2\alpha_P(t)-1},$$

where  $t$  is the momentum transferred between the initial proton and its final state fragment. Since  $|t|$  is small in the bulk of these events, the approximate  $x$ -independence of the fraction  $F_2^{LRG}/F_2$  corresponds to  $\alpha_P(0) \approx 1$  as inferred from hadronic phenomenology [3]. Thus the probability for these large rapidity gap events is proportional to  $\exp(-c\Delta y)$  with  $c = 1 - \alpha_P(0) \approx 0$ , so we do not get a substantial decrease in the number of rapidity-gap events as the rapidity gap is increased. If Pomeron exchange factorizes in the cross channel, which is consistent with hadron phenomenology [3] (but is *not* yet confirmed in deep inelastic scattering and which furthermore cannot be understood within the context of perturbative QCD), then the structure function of the Pomeron,  $F_2^P(\beta, Q)$ , may be extracted from the large-rapidity-gap events at HERA.

Bjorken, Brodsky and Lu [4] considered a kinematical configuration in which  $e^+e^-$  goes to two low-mass clusters, as illustrated in Fig.2. We believe

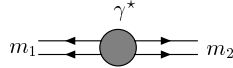


Figure 2: Events with two low-mass clusters in  $e^+e^-$  annihilation (viewed in the centre-of-mass frame).

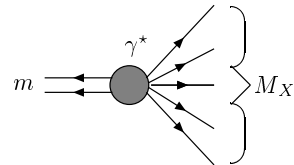


Figure 3: Large-rapidity-gap configuration in  $e^+e^-$  annihilation (again viewed in the centre-of-mass frame).

that a closer analogue in  $e^+e^-$  annihilation to the HERA large rapidity-gap observations (in which  $Q$  and  $M_X$  are both large, with  $t$  fixed) is provided by the kinematical configuration illustrated in Fig. 3, where only one of the two produced clusters is required to have a small mass ( $m$ ), while the other is allowed to have a large mass,  $M_X \sim \mathcal{O}(Q)$ . The small-mass cluster looks like a colour-singlet jet with scaled energy fraction,  $x_3 = 1 - M_X^2/Q^2$ . In QCD perturbation theory, the deep-inelastic structure function at low  $x$  is dominated by photon-gluon fusion as illustrated in Fig. 4. The lowest-order perturbative contribution to large rapidity-gap deep-inelastic events involves two gluon exchanges as illustrated in Fig. 5. The standard three-

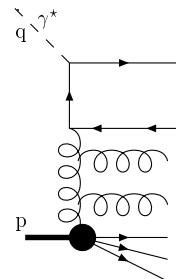


Figure 4: Photon-gluon fusion.

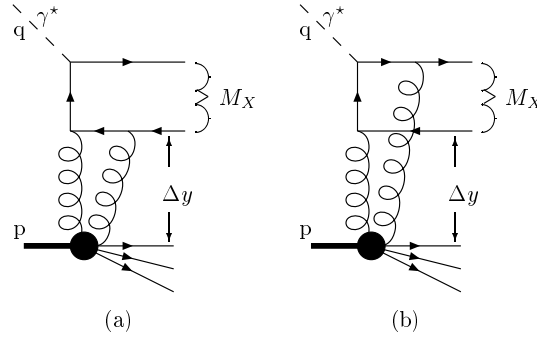


Figure 5: Leading-order contribution to large-rapidity-gap events in deep-inelastic scattering.

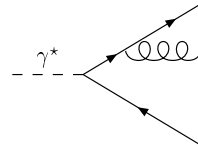


Figure 6: Standard three-jet events in  $e^+e^-$  annihilation.

jet final state of Fig. 6 is the closest  $e^+e^-$  analogue of the photon-gluon fusion diagram of Fig.4. The lowest-order perturbative contributions to the colour-singlet cluster production in  $e^+e^-$  annihilation are those shown in Fig. 7, where Fig.7(a), in which a ‘glueball’ is produced, is very similar to the deep-inelastic two-gluon exchange diagram of Fig. 5.

Here we make a few pertinent comments about the leading perturbative contribution to deep-inelastic large rapidity-gap events due to the diagrams shown in Fig.5. If one calculates the absorptive part of these diagrams, then the on-shell condition for the cut fermion line forces one of the exchanged gluons to have zero longitudinal momentum. Furthermore, an explicit calculation [5] shows that the amplitude is indeed dominated by the kinematic regime where one of the gluons is much more energetic than the other. As we shall see later, an analogous infrared singularity also dominates the contribution of the graphs of Fig. 7(a) to colour-singlet jet production in  $e^+e^-$  annihilation. Moreover, in the case where one of the gluons in Fig. 5 is soft, the quark-antiquark system appears as a colour dipole, and the contributions from Figs. 5(a) and (b) cancel each other if the quark and antiquark have

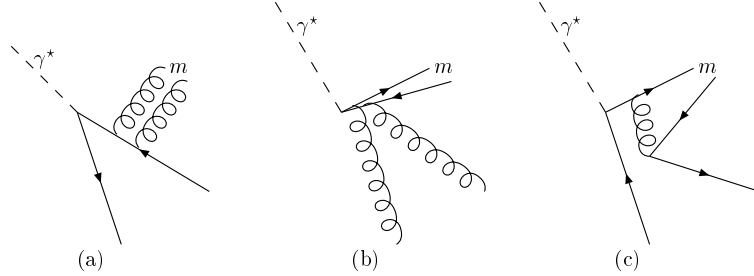


Figure 7: Single low-mass cluster events in  $e^+e^-$  annihilation. For each type of event we display only one of the possible Feynman graphs.

large transverse momentum (and therefore occupy a small region of impact-parameter space). Thus the process is dominated by the low-transverse-momentum kinematic region in which the fermions are almost parallel to the incoming photon or hard gluon (this is the aligned jet model [6]). In this kinematic regime the internal quark is close to its mass shell, so that the graph cannot be determined purely from perturbation theory. An infrared scale, presumably of order  $\Lambda_{QCD}$ , is introduced by the non-perturbative dynamics, and it is because of this scale that the probability for large-rapidity-gap events is not exponentially suppressed with rapidity gap, as would be expected from a simple dimensional analysis as in naive perturbation theory. Of course, since we are looking at events at low  $x$ , the two gluons of Fig. 5 constitute the Born term of the complete BFKL ladder, giving rise to a “hard” Pomeron with an intercept considerably above unity. Nevertheless, we expect that the above discussion will hold when the complete ladder is taken into account. The non-perturbative mechanism that gives rise to this infrared scale that prevents the large-rapidity-gap events from being exponentially suppressed, is the same mechanism that reduces the intercept of the “soft” Pomeron, which controls hadron diffractive processes at low momentum transfer, to a value close to unity.

In this paper we show that the glueball production diagrams of Fig. 7(a), when suitably regulated in the infrared region, do *not* give a large cross-section for large-rapidity-gap events in  $e^+e^-$  annihilation. Specifically, in the limit  $m/\sqrt{s}$  fixed,  $s \rightarrow \infty$ , we find a cross section that falls as  $1/s$ , relative to the normal three-jet cross section. This is the scaling law that one would normally expect from dimensional analysis for the production of an isolated fixed-mass cluster, but corresponds to a suppression of large-

rapidity-gap events in  $e^+e^-$  annihilation. The reason for this difference from deep-inelastic-scattering is that, after the regularisation of the (logarithmic) infrared divergence by some suitable wavefunction or fragmentation function, the events under consideration *can* be determined in perturbation theory, and the infrared scale which is so important in the case of deep-inelastic scattering does not play a significant role in the  $e^+e^-$ -annihilation case, even though the relevant diagrams can be thought of as the production of a “Pomeron” in the s-channel.

The layout of this paper is as follows. In Section 2 we review the different kinematics of deep-inelastic scattering and  $e^+e^-$  annihilation, discuss the evaluation of our basic perturbative QCD diagrams in Fig. 7, and relate our calculation to that of ref.[4]. Next, in Section 3, we discuss the treatment of the infrared divergence in the cross-section, comparing and contrasting the  $e^+e^-$  situation with the use of naive Pomeron structure functions in deep-inelastic scattering, and introducing an infrared cutoff derived from a physical picture of a typical glueball wavefunction. Our main results are presented in section 4, including the dependences of the isolated cluster cross section on this wavefunction cutoff, on the cluster mass, on the rapidity gap with the rest of the event, and on the centre-of-mass energy,  $\sqrt{s}$ . Section 5 includes a discussion of our results and the prospect for detecting large-rapidity-gap events in  $e^+e^-$  annihilation. An Appendix presents the differential cross section for the production of two quarks and two antiquarks in a suitable form for our study.

## 2 The Parton-Level Calculation

In  $e^+e^-$  annihilation, the equivalent of the “pomeron” exchanged in the  $t$ -channel in a deep-inelastic scattering event is the production of a colour-singlet gluon cluster or a glueball in the case where the cluster consists of just one particle. One of the Feynman diagrams for this process in leading order in perturbation theory is shown in Fig. 7(a), in which the two gluons are constrained to be in a colour singlet and to have fixed invariant mass,  $m$ , which is much smaller than the total centre-of-mass energy  $\sqrt{s}$ .

A similar process was considered in ref.[4]. However, there the authors constrained both the pairs of particles to have small invariant mass, thereby greatly reducing the available phase-space and consequently reducing the

cross-section. In our case we will be concerned with the differential cross section with respect to  $m^2$ , subject to the requirement that there must be a minimum rapidity gap,  $\Delta y$  between the gluon cluster and either of the fermion jets.

$$\Delta y = \min(\Delta y_1, \Delta y_2) \quad (2.1)$$

If the quark (antiquark) jet  $i$ , ( $i = 1, 2$ ) makes an angle  $\theta_i$  with the direction of the gluon cluster, then the rapidity gap between that jet and the gluon cluster is (up to corrections of order  $m^2/s$ )

$$\Delta y_i = \ln \left( \frac{\sqrt{s}}{m} \right) + \ln x_3 - \frac{1}{2} \ln \left( \frac{1 + \cos \theta_i}{1 - \cos \theta_i} \right) \quad (2.2)$$

where the variable  $x_3$  introduced in ref. [7] is the fraction of available energy ( $\sqrt{s}/2$ ) of the gluon cluster. We may rewrite this in terms of the energy fraction,  $x_i$  carried by the  $i^{\text{th}}$  fermion jet, using the relation

$$(1 - \cos \theta_i) = \frac{2(x_i + x_3 - 1)}{x_i x_3}$$

For very large rapidity gaps, the fermion jets are both forced to be almost in the opposite direction to the gluon cluster and in this limit we recover the results of ref. [4].

In  $e^+e^-$ -annihilation, the kinematic quantity which is analogous to the invariant mass of the quark-antiquark pair produced in the photon-pomeron collision is given by

$$M_X^2 = s(1 - x_3) \quad (2.3)$$

The fact that we wish to allow this to be of order  $\sqrt{s}$  means that we stay away from the  $x_3 \rightarrow 1$  limit. On the other hand, as can be seen from Eq.(2.2), requiring a very large rapidity gap forces  $x_3$  to be close to unity. As we shall see in Section 4, the production rate drops rapidly in this limit.

In more detail, if we assign momenta  $p_1$  and  $p_2$  to the outgoing quark and antiquark and momenta  $p_3, p_4$  to the two gluons, then we fix

$$s_{34} = m^2 \quad (2.4)$$

and identify

$$s_{134} = s(1 - x_2) \quad (2.5)$$

and

$$s_{234} = s(1 - x_1) \quad (2.6)$$

where

$$s_{ij} = (p_i + p_j)^2$$

and

$$s_{ijk} = (p_i + p_j + p_k)^2$$

This enables us to select the required region of phase space. One further quantity that we shall need to identify is  $z$ , the fraction of the energy of the gluon cluster carried by one of the gluons. Up to corrections of order  $m^2/s$ , this is given by

$$z \approx \frac{s_{13}}{s_{13} + s_{14}} \approx \frac{s_{23}}{s_{23} + s_{24}} \quad (2.7)$$

The squared matrix element for the processes shown in Figs. 7 (a) and (b) are given in the Appendix of ref.[8]. What we need to do is to identify the relevant colour factors for the process we are considering, and perform a (numerical) integral over the required region of phase space. In ref.[8] a summation was performed over all final-state helicities, in particular over the final-state helicities of the gluons. If the gluon cluster consists of a single glueball, we might wish to project out a particular linear combination of helicity states which make up the spin of the glueball. In the absence of any concrete information about what spin states would be expected to dominate for particular gluon cluster masses we do not take this into consideration, and we assume that summing over all gluon helicity states does not introduce significant errors.

In order to project out the colour-singlet part of the gluons (of colours  $a$  and  $b$ ) we apply

$$\frac{\delta_{ab}}{\sqrt{8}}$$

to the matrix element. Thus the colour factor for the squared matrix element becomes

$$(\tau^a \tau^b)_{ij} \frac{\delta_{ab}}{\sqrt{8}} (\tau^c \tau^d)_{ij} \frac{\delta_{cd}}{\sqrt{8}} = \frac{C_F^2}{8} \delta_{ij} \delta_{ij} \quad (2.8)$$

where the  $\tau^a$  are the colour matrices and  $C_F = 4/3$  is the quadratic Casimir in the fundamental representation. The factor  $\delta_{ij} \delta_{ij}$  is present in the tree-level total cross section to which we normalise our calculations. Thus the rule is that we set  $C_A = 0$  in the formulae given in [8] and divide by a factor of 8.

For the process shown in Fig. 7(b) the colour factor is identical. The difference is that we now set

$$s_{12} = m^2 \quad (2.9)$$

and make similar changes ( $1 \leftrightarrow 3$ ,  $2 \leftrightarrow 4$ ) in the rest of the kinematics.

For the process shown in Fig. 7(c) the complete squared matrix element was not given in [8], since some of the interference terms vanish when integrated over phase-space by virtue of Furry's theorem. However, this cancellation only occurs if the phase-space integration is performed to find the differential cross-section with respect to a variable which is symmetric in all the final state particles. This is not the case in the process we are considering, since we require that two of the fermions should have a small invariant mass. The squared matrix element for the production of two quark-antiquark colour signlet pairs each with flavours a and b (including the colour factor) is given in the Appendix. It is necessary to perform a sum over all possible flavours and normalise to the total hadronic cross section as discussed in ref.[4].

Requiring a large rapidity gap eliminates the region of phase space where one finds collinear divergences, in which a gluon runs parallel to a fermion line. However, we do not eliminate infrared divergences which occur when one of the gluons becomes soft, i.e. when the fraction of energy,  $z$ , of the gluon cluster, carried by one of the gluons goes to zero or unity. This introduces a logarithmic divergence in the phase-space integral. Such divergences are regularized by the fragmentation of the two gluons into hadrons, or by a wavefunction in the case of a single glueball state. The fragmentation function or wavefunction must vanish when  $z = 0$  or  $z = 1$ . It is to a discussion of this wavefunction that we now turn.

### 3 The Wavefunction

One example of a possible form for the two-gluon squared wave function of a glueball would be

$$|\psi(z)^2| = \mathcal{N}z(1-z) \quad (3.1)$$

where  $\mathcal{N}$  is a normalization factor and  $z$  and  $(1-z)$  are the longitudinal momentum fractions of the constituent gluons in the infinite-momentum frame. A similar form has often been discussed in connection with the deep-inelastic

Pomeron structure function, and it has the desirable feature of removing the infrared singularity as  $z \rightarrow 0, 1$ . However, the physical intuition behind this choice is not very clear, and we prefer to use a wave function that is better motivated by simple ideas about the physical composition of a glueball.

Two gluons with negligible mass, equal and opposite transverse momenta  $\underline{k}_T$ , and longitudinal momentum fractions  $z$  and  $(1 - z)$  in the infinite-momentum frame, have a combined invariant mass-squared

$$m^2 = \underline{k}_T^2 \left( \frac{1}{z} + \frac{1}{1-z} \right) \quad (3.2)$$

The corresponding transverse size  $R_T$  is given by

$$R_T^2 = \frac{1}{\underline{k}_T^2} = \frac{1}{z(1-z)} \frac{1}{m^2} \quad (3.3)$$

We choose the following plausible form for the glueball wave function

$$|\psi(R_T^2)| \approx \exp \left( \frac{-R_T^2}{b^2} \right) \quad (3.4)$$

for some size parameter  $b$ . The corresponding squared longitudinal-momentum wave function is

$$|\psi(z)^2| = \mathcal{N} \exp \left[ -\frac{1}{m^2 b^2 z(1-z)} \right] \quad (3.5)$$

where  $\mathcal{N}$  is a normalization factor. We note that this also regulates the infrared divergences from the parton-level differential cross-section when  $z \rightarrow 0, 1$ . Possible choices of  $b$  for different glueball masses  $m$  will be discussed in the next section.

Clearly, other choices of wave function are possible, which injects an uncontrolled infrared sensitivity into our results. Nevertheless, we believe that the results we present in later sections reflect qualitatively what might be expected with any “reasonable” choice of wave function.

## 4 Results

In this section we present our main results.

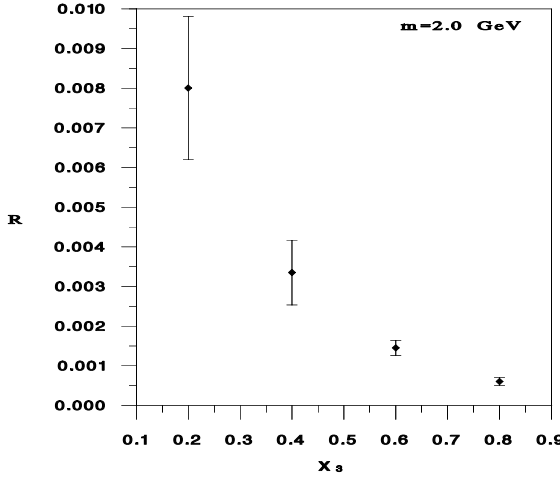


Figure 8: Graph of  $R$  defined in Eq.(4.1) as a function of  $x_3$ . The error bars show the variation as  $x_1$  (or  $x_2$ ) is varied keeping  $x_3$  fixed.

We begin by demonstrating that the cross section for the production of a low-mass gluonic cluster and two fermion jets depends mainly on the energy fraction of the gluon cluster  $x_3$  and rather less on  $x_1$  ( $x_2$ ), <sup>†</sup> the energy fractions of the fermion jets. We show this in Fig. 8, in which the quantity  $R$  is the ratio

$$R = \frac{d^3\sigma}{dx_1 dx_2 dm^2} / \frac{d^2\sigma_0}{dx_1 dx_2} \quad (4.1)$$

where  $d^2\sigma_0/dx_1 dx_2$  is the tree level cross section for the production of three-jets calculated in ref. [7]. We have taken the gluon cluster mass,  $m$ , to be 2  $GeV$  and the centre-of-mass energy equal to  $M_Z$ . The infrared divergence which occurs when one of the gluons becomes soft is regulated simply by demanding that all invariant masses should be greater or equal to  $m$ . The graph clearly shows a substantial dependence on  $x_3$  and a rather modest dependence on  $x_1$  ( $x_2$ ). Since the production rate is dominated by the region of phase space where one of the gluons is soft, this is at first a rather surprising result, since we would expect that an extra soft gluon would yield an  $x_3$  dependence which was not very different from the three-jet  $x_3$  dependence,

---

<sup>†</sup>We remind the reader that  $x_1, x_2, x_3$  are related by  $x_1 + x_2 + x_3 = 2$

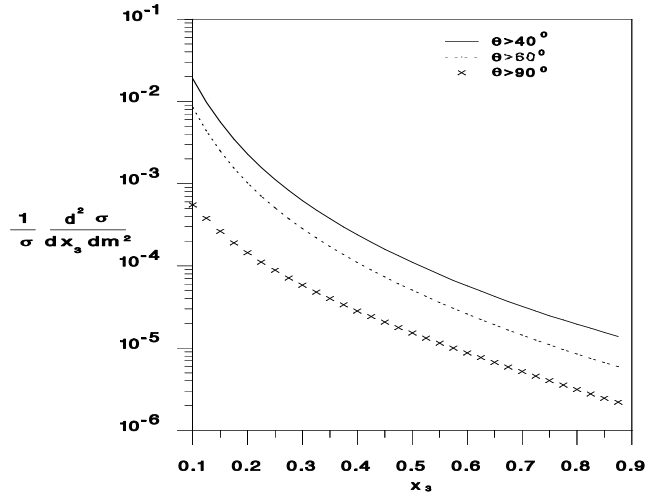


Figure 9: Graph of differential cross section against  $x_3$  for different minimum opening angles between the gluon cluster and the fermion jets.

so that one might have expected that this ratio should be approximately constant. However, as explained above, this is *not* the case for deep-inelastic scattering, in which the ratio of the two-gluon to one-gluon exchange is very sensitive to the transverse momentum of the fermion pair. The  $x_3$  dependence that we see here is the analogue of this effect in  $e^+e^-$  annihilation.

We now turn to the more realistic case of the perturbative prediction of events with a low-mass gluonic cluster in which the infrared divergence is regulated by a wavefunction as discussed in Section 3. We take as the default value of the “average impact parameter”  $b = 2 \text{ GeV}^{-1}$ , and again the cluster mass is  $2 \text{ GeV}$ . We start by showing distributions not with a minimum rapidity gap, but with a minimum opening angle  $\theta$  between the gluon cluster and either of the fermion jets. Such opening angles are more directly controlled experimentally. These opening angles are related to the rapidity gap, but the exact relation between the opening angle and the rapidity gap depends on the gluon cluster energy fraction  $x_3$ .

The results are shown in Fig. 9, where we have taken three different minimum opening angles. The substantial decrease in differential cross section

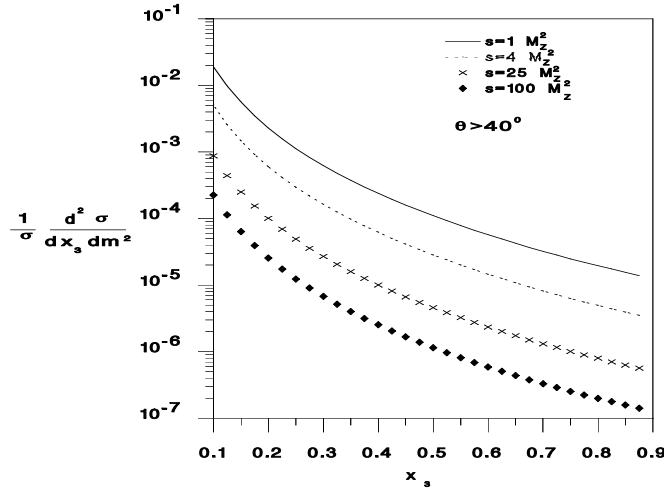


Figure 10: Graph of differential cross section against  $x_3$  for different centre-of-mass energies.

as the opening angle is increased is indicative of a substantial decrease with increasing rapidity gap. We emphasize this point further in Fig. 10, where we fix the minimum opening angle to be  $40^\circ$ , but allow the centre-of-mass energy

to take values  $2 M_Z$ ,  $5 M_Z$  and  $10 M_Z$  as well as  $M_Z$ . The sharp decrease in differential cross section goes like  $1/s$ , as expected from dimensional analysis, which means that events with a low-mass gluon cluster will be even more difficult to detect in higher-energy  $e^+e^-$  machines in the future.

Next we turn to Fig. 11, where we plot the differential cross-section, again against  $x_3$ , for different values of the minimum rapidity gap. A behaviour  $\sim \exp(-c\Delta y)$ , with  $c \approx 2$  can be seen. Once again, this is the  $1/s$  behaviour that one would expect from dimensional analysis, which is therefore expected to hold (up to logarithmic corrections) in any perturbative calculation. In Fig. 12 we show the plot the other way around, i.e., for fixed gluon cluster energy fraction  $x_3$  we plot the differential cross-section with respect to  $m^2$  and  $\Delta y$ . The same fall-off with the length of the rapidity gap can be seen. It is worth noting in both of these graphs that there is a sharp cutoff in  $x_3$  for

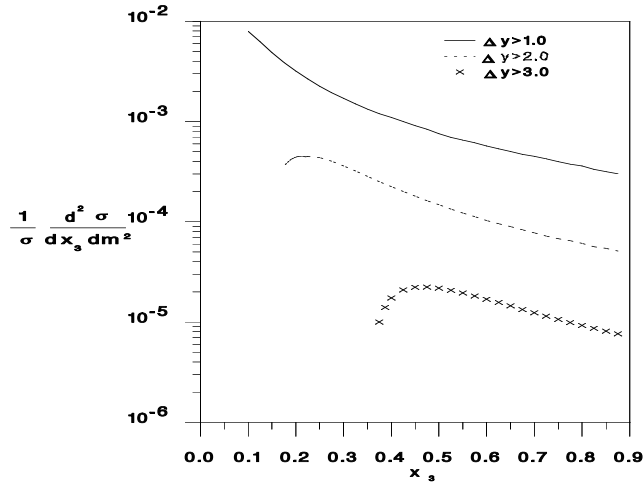


Figure 11: Graph of differential cross section against  $x_3$  for different minimum rapidity gaps.

a given rapidity gap. This is because events with the required rapidity gap are excluded by the kinematics if the energy of the gluon cluster is below a certain value.

In order to demonstrate the dependence on the other two parameters, namely the mass  $m$  of the gluonic cluster and the “average impact parameter”  $b$  used in the wavefunction, we plot in Figs. 13 and 14 the differential cross-section with the minimum rapidity gap (set to  $\Delta y = 1.5$ ) for different values of  $m$  and  $b$  respectively. As expected, if we increase the cluster mass  $m$  there is more phase space available for the events, and so the differential cross-section is increased. As  $b$  is increased, the wavefunction (see Eq.(3.5)) provides a suppression only for fractional gluon energy  $z$  closer to the endpoints  $z = 0$  and  $z = 1$ . We therefore pick up more of the infrared-enhanced differential cross-section and this explains the increase seen in Fig.14.

Finally, we look at the contributions to a colour-singlet cluster formation from quark-antiquark pairs. There are two possibilities shown in Figs. 7(b) and (c). In one case the other two jets are gluonic - here we consider the same matrix element given in the Appendix of ref. [8], but in a different region of

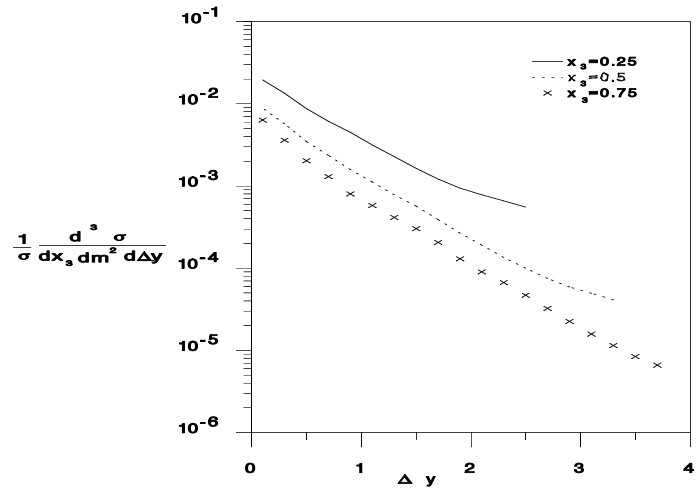


Figure 12: Graph of differential cross section against minimum rapidity gap for various different values of  $x_3$ .

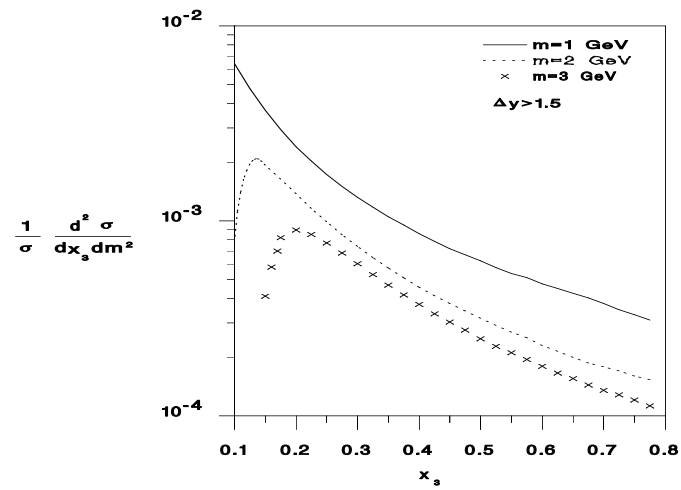


Figure 13: Graph of differential cross section  $x_3$  for different values of  $m$ .

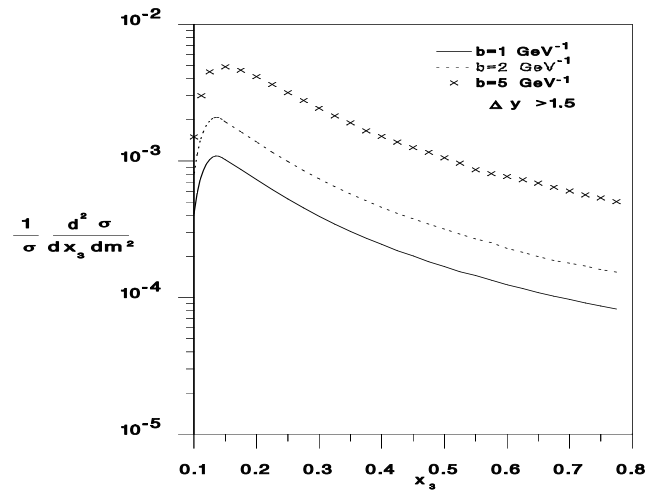


Figure 14: Graph of differential cross section  $x_3$  for different values of  $b$ .

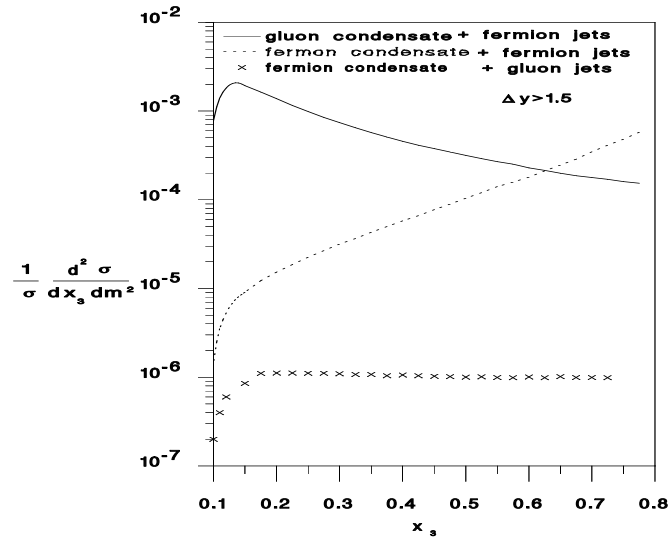


Figure 15: Graph of differential cross section  $x_3$  showing gluon-cluster and fermion-cluster contributions.

phase space. In the other case the other jets are also fermionic. The squared matrix element for this process is given in the Appendix. The results are shown in Fig. 15, in which we have taken the default values,  $m = 2 \text{ GeV}$ ,  $b = 2 \text{ GeV}^{-1}$  and a rapidity-gap of 1.5. We see that, apart from large  $x_3$  where the gluon cluster contribution is small, both the fermion cluster contributions are negligible and do not show the same strong dependence on  $x_3$  as the gluon cluster. The reason for this is that there is no infrared-enhanced contribution. In the first case, where the unobserved jets are gluonic, since the quark and antiquark are almost parallel the soft gluon insertion cancels between the insertion on the quark and antiquark line (in a similar way to the cancellation at large  $p_\perp$  in deep-inelastic scattering). In the case of a four-fermion final state, there is no infrared divergence when we force the quark and antiquark with the same flavours to go into different colour-singlet clusters.

In general, the differential cross-sections we have found are very small and cannot be observed at present. However, they are considerably larger than those predicted in ref. [4], which is hardly surprising since in our case there is much more phase space available.

## 5 Discussion

We have considered in this paper the possible rate of large-rapidity-gap events in  $e^+e^-$  annihilation due to the lowest-order perturbative QCD diagrams shown in Fig. 7. The kinematical configuration we study (Fig. 3) is similar to that of the rapidity-gap events observed at HERA (Fig. 1), and more general than the case of two low-mass clusters considered previously (Fig. 2). Correspondingly, we find a cross-section that is considerably larger than that estimated in Ref. [4]. Taking the ratio  $R$  of colour-singlet cluster events to conventional three-jet events (Fig. 6), we find that  $R$  depends sensitively on the scaled gluon energy  $x_3$ , but less sensitively on the scaled  $q$  and  $\bar{q}$  energies  $x_1, x_2$  (Fig. 8). As we show in Figs. 9, 11 and 12, the cross-section falls as the angle (rapidity) gap between the colour-singlet cluster and the rest of the event is increased: there is no indication of a “rapidity plateau” as known in hadron-hadron and  $ep$  collisions. Correspondingly, we see in Fig. 10 that the cross section falls as the centre-of-mass energy increases. This is not surprising, since an infrared cutoff scale appears via the fixed mass  $m$  of the colour-singlet cluster considered: the  $m$ -dependence of the cross section is shown in Fig. 13. As seen in Fig. 15, most of the colour-singlet clusters are

digluons. Our cross-section estimates are based upon a particular form for the infrared cutoff discussed in Section 3: the sensitivity to the glueball wavefunction size parameter  $b$  is illustrated in Fig. 14. However, other choices of the form of infra-red cut-off are possible, and the uncertainty in the cross-section estimates could well be larger than suggested by Fig. 14. Nevertheless, we find that the cross section for large-rapidity-gap events probably lies below the experimental sensitivity of, for example, a recent search by the ALEPH collaboration [9]. The fact that the calculated cross section falls with the centre-of-mass energy, as seen in Fig. 10, means that this situation will worsen at higher energies (e.g., LEP II, NLC/JLC/CLIC), despite the larger phase space.

We therefore conclude that the prospects for observing large-rapidity-gap events in  $e^+e^-$  annihilation are dim, at least in the context of perturbative QCD. This reflects the different dynamical conditions in the time-like region, namely colour-singlet production  $e^+e^-$  annihilation, and the space-like region, namely crossed-channel colour-singlet exchange in hadron-hadron or  $ep$  collisions. One has to be “lucky” to produce two real gluons close together in phase space, with none radiated elsewhere, whereas it is relatively “easy” for a long-range Coulomb gluon field to bleach colour over a large rapidity gap.

## 6 Acknowledgements:

The authors are grateful to Michael Schmitt for useful conversations.

One of us (J.E.) would like to thank the Physics Department at Southampton University for its hospitality while part of this work was done.

## 7 Appendix

In this Appendix we present the tree-level result for the differential cross section  $d\sigma$  for an  $e^+e^-$  pair with centre-of-mass energy  $\sqrt{s}$  to go into a colour-singlet pair consisting of a quark with momentum  $p_1$  and flavour  $a$  (charge  $Q_a$ ) plus an antiquark with momentum  $p_2$  and flavour  $b$  (charge  $Q_b$ ), and a colour singlet consisting of a quark with momentum  $p_3$  and flavour  $b$  plus an antiquark with momentum  $p_4$  and flavour  $a$ .

Defining

$$s_{ij} = (p_i + p_j)^2$$

$$s_{ijk} = (p_i + p_j + p_k)^2$$

we have (normalising with respect to the leading-order total cross-section,  $\sigma_0$ )

$$\begin{aligned} \frac{1}{\sigma_0} d\sigma = & \frac{1}{\sum_a Q_a^2} \frac{C_F^2}{3} \left( \frac{\alpha_s}{2\pi} \right)^2 \frac{1}{4s^2} \int ds_{134} \int ds_{234} \int ds_{34} \theta(s_{134}s_{234} - ss_{34}) \\ & \theta(s_{34} + s - s_{134} - s_{234}) \int_0^1 dv \frac{1}{\pi} \int_0^\pi d\phi [f(s_{12}, s_{13}, s_{14}, s_{23}, s_{24}, s_{34}) + \\ & f(s_{34}, s_{24}, s_{14}, s_{23}, s_{13}, s_{12}) + f(s_{34}, s_{13}, s_{23}, s_{14}, s_{24}, s_{12}) + \\ & f(s_{12}, s_{24}, s_{23}, s_{14}, s_{13}, s_{34})] \end{aligned} \quad (\text{A.1})$$

where

$$v = \frac{s_{24}}{s_{124} - s_{34}},$$

$\phi$  is the azimuthal angle of the 34 system relative to the 12 plane, and

$$\begin{aligned} f(s_{12}, s_{13}, s_{14}, s_{23}, s_{24}, s_{34}) = & (Q_a^2 + Q_b^2) \left[ \frac{1}{s_{14}^2 s_{134}^2} (s_{12}s_{13}s_{14} + s_{12}s_{13}s_{34} \right. \\ & - s_{12}s_{34}^2 - s_{13}^2 s_{24} + s_{13}s_{14}s_{23} + 2s_{13}s_{23}s_{34} + s_{13}s_{24}s_{34} + s_{14}s_{23}s_{34} \\ & + s_{14}s_{24}s_{34}) \\ & + \frac{1}{2s_{14}^2 s_{134} s_{234}} \left( -s_{12}^2 s_{34} + s_{12}s_{13}s_{24} + s_{12}s_{13}s_{34} + s_{12}s_{14}s_{23} - 2s_{12}s_{23}s_{34} \right. \\ & + s_{12}s_{24}s_{34} - s_{12}s_{34}^2 - s_{13}^2 s_{24} + s_{13}s_{14}s_{23} - 2s_{13}s_{23}s_{24} - s_{13}s_{24}^2 + s_{13}s_{24}s_{34} \\ & \left. \left. + 2s_{14}^2 s_{23} + 2s_{14}s_{23}^2 + s_{14}s_{23}s_{24} + s_{14}s_{23}s_{34} \right) \right] \\ & - Q_a Q_b \frac{1}{4s_{14}s_{23}} \left[ \frac{1}{s_{124}s_{123}} \left( -s_{12}^2 s_{34} - 4s_{12}s_{13}s_{14} - 5s_{12}s_{13}s_{24} \right. \right. \\ & \left. \left. - 3s_{12}s_{14}s_{23} - 2s_{12}s_{14}s_{34} - 4s_{12}s_{23}s_{24} - 2s_{12}s_{23}s_{34} - 4s_{12}s_{24}s_{34} \right) \right] \end{aligned}$$

$$\begin{aligned}
& -2s_{12}s_{34}^2 - 2s_{13}s_{14}s_{24} - 2s_{13}s_{23}s_{24} - s_{13}s_{24}^2 + 2s_{13}s_{24}s_{34} + 2s_{14}^2s_{23} \\
& + 2s_{14}s_{23}^2 + s_{14}s_{23}s_{24} + 2s_{14}s_{23}s_{34} \Big) \\
& + \frac{1}{s_{124}s_{234}} \left( -2s_{12}s_{13}s_{34} + 2s_{12}s_{14}s_{34} + 4s_{12}s_{23}s_{24} + 2s_{12}s_{23}s_{34} \right. \\
& + 6s_{12}s_{24}s_{34} + 2s_{13}s_{24} - 2s_{13}s_{14}s_{23} + 2s_{13}s_{14}s_{24} + 2s_{13}s_{23}s_{24} \\
& \left. + 2s_{13}s_{24} - 2s_{14}^2s_{23} - 2s_{14}s_{23}^2 + 2s_{14}s_{23}s_{24} + 4s_{14}s_{24}s_{34} \right) \Big] \quad (A.2)
\end{aligned}$$

The terms proportional to  $(Q_a^2 + Q_b^2)$  coincide with the quantity  $D$  of [8] (Eq.B.6), with the colour factor  $T_R$  replaced by  $C_F/3$ . The other terms are the class  $F$  terms (see Table 2 of ref.[8]), which were not given explicitly in ref.[8].

## References

- [1] H. Cheng and C.Y. Lo, Phys. Rev. **D15** (1977) 2959  
L.L. Frankfurt and V.E. Sherman, Sov. J. Nucl. Phys. **23** (1976) 581  
A.L. Mason, Nucl. Phys. **B104** (1976) 141  
L.N. Lipatov, Sov. J. Nucl. Phys. **23** (1976) 338  
L. Tyburski, Phys. Rev. **D13** (1976) 1107  
E.A. Kurayev, L.N. Lipatov and V.S. Fadin, Sov. Phys. JETP **44** (1976) 443; **45** (1977) 199  
Y.Y. Balitsky and L.N. Lipatov, Sov. J. Nucl. Phys. **28** (1978) 822
- [2] V.N. Gribov and L.N. Lipatov, Sov. J. Nucl. Phys. **15** (1972) 675  
G. Altarelli and G. Parisi, Nucl. Phys. **B226** (1977) 218  
L. Dokshitzer, Sov. Phys. JETP **46** (1977) 64
- [3] A. Donnachie and P.V. Landshoff, Phys. Lett. **B296** (1992) 227
- [4] J.D. Bjorken, S.J. Brodsky and H.J. Lu, Phys. Lett. **B286** (1992) 153
- [5] J. Bartels, H. Lotter and M. Wüsthoff, DESY preprint 94-245 (1995)
- [6] J.D. Bjorken, Proc. 1971 Int. Symp. on Electron and Photon Interactions, Cornell, ed. N.B. Mistry (Cornell, Ithaca, 1971) p.281  
and in Current Induced Reactions, Hamburg 1975, eds. J.G. Körner, G. Kramer and D. Schildknecht (Springer, 1975) p.93
- [7] A. De Rújula, J. Ellis, E.G. Floratos and M.K. Gaillard, Nucl. Phys. **B138** (1978) 387
- [8] R.K. Ellis, D.A. Ross and A.E. Terrano, Nucl. Phys. **B178** (1981) 421
- [9] M. Schmitt, private communication.